

# Effectiveness of a nonlinear energy sink in the control of an aeroelastic system

Youssef Bichiou · Muhammad R. Hajj ·  
Ali H. Nayfeh

Received: 3 November 2015 / Accepted: 21 June 2016 / Published online: 1 July 2016  
© Springer Science+Business Media Dordrecht 2016

**Abstract** The effectiveness of the nonlinear energy sink in controlling the limit cycle oscillations of a nonlinear aeroelastic system is assessed. The system consists of a rigid airfoil elastically mounted on linear and nonlinear springs. The coupled equations of the airfoil and sink are derived using Lagrange's equations. The nonlinear quasi-steady aerodynamics are used to model the aerodynamic loads. Parameters including the mass and placement of the passive controller are varied in order to test its efficiency in suppressing undesirable aeroelastic behavior under varying conditions. The nonlinear normal form governing the responses of the airfoil and the energy sink is derived. The contribution of the aerodynamic, structural and sink nonlinearities to the type of instability is quantified. The results show that the nonlinear energy sink has a limited impact on the system's response in terms of effectively delaying the onset of flutter, changing the type of instability or reducing the amplitude of the limit cycle oscillations.

**Keywords** Nonlinear energy sink · Flutter · Normal form · Hopf bifurcation

## Abbreviations

$h$	Plunge motion
$\theta$	Pitch motion
$y_2$	NES motion
$\alpha_0$	Preset angle of attack
$\alpha_{\text{eff}}$	Effective angle of attack
$m_1$	Mass of the airfoil
$m_2$	Mass of the NES
$e$	Position of the center of gravity relatively to the elastic axis
$d$	Position of the NES relatively to the elastic axis
$I_{cg}$	Mass moment of inertia of the airfoil relatively to the center of gravity
$k_{h_0}$	Airfoil linear plunging stiffness
$k_{h_1}$	Airfoil quadratic plunging stiffness
$k_{h_2}$	Airfoil cubic plunging stiffness
$C_h$	Airfoil plunging motion viscous damping coefficient
$k_{\theta_0}$	Airfoil linear pitching stiffness
$k_{\theta_1}$	Airfoil quadratic pitching stiffness
$k_{\theta_2}$	Airfoil cubic pitching stiffness
$C_\theta$	Airfoil pitching motion viscous damping coefficient
$k_{n_0}$	NES linear plunging stiffness
$k_{n_1}$	NES quadratic plunging stiffness
$k_{n_2}$	NES cubic plunging stiffness
$C_{y_2}$	NES plunging motion viscous damping coefficient

Y. Bichiou · M. R. Hajj (✉) · A. H. Nayfeh  
Department of Biomedical Engineering and Mechanics,  
MC 0219, Virginia Tech, Blacksburg, VA 24061, USA  
e-mail: mhajj@vt.edu

A. H. Nayfeh  
e-mail: anayfeh@vt.edu

$L$	Aerodynamic lift force
$M$	Aerodynamic moment
$b$	Semi-chord
$C_{l_\alpha}$	Lift coefficient
$C_{m_\alpha}$	Moment coefficient
$c_s$	Nonlinear aerodynamic coefficient
$U$	Freestream velocity
$\rho$	Air density

## 1 Introduction

Flutter control and suppression of limit cycle oscillations have been objectives of many investigations of aeroelastic systems. The interest is in expanding the flight boundary and enhancing aircraft performance. Furthermore, successful robust control strategies can be used to reduce the number of required flight tests for different configurations. Different strategies, including active and passive controls, have been proposed to increase the flutter speed or suppress limit cycle oscillations. The use of active control strategies requires external actuators and sensors. These requirements are not needed in passive control strategies. This is an important advantage in terms of keeping the payload to a minimum and avoiding issues associated with control surfaces.

We focus in this work on one mechanism that has been proposed as a passive control strategy, namely the nonlinear energy sink (NES), to suppress or reduce the amplitude of limit cycle oscillations of aeroelastic systems. The NES has been proposed to suppress the vibrations of different mechanical systems. It is composed of a secondary system with a nonlinear stiffness that is attached to the main system. The idea behind it is to pump the energy of the main system to the NES and, as such, limit the amplitude of its motion. One advantage of having a nonlinear stiffness is that the passive pumping of energy would take place irrelevant of the frequency of the motion of the main system. Although successful in some applications, the NES has been shown to have some shortcomings in terms of yielding multiple solutions and practicality especially when it comes to specific types of instabilities. Lee et al. [1] showed that the NES causes a delay in flutter and a reduction in the amplitudes of oscillations. Jiang et al. [2] experimentally and theoretically investigated the dynamics of an NES that is weakly coupled to a linear structure that was harmonically forced. They

determined that, due to the nonlinearity, the NES can vibrate with any mode of the primary system. Malatkar and Nayfeh [3] investigated the system considered by Jiang et al. [2] and showed that multiple solutions for undamped or slightly damped linear subsystems exist. They also showed that, for lightly damped subsystems, the NES increases the amplitude of oscillations when increasing the mass. Recently, Mehmood et al. [4] investigated the use of the NES to suppress the vortex-induced vibrations of a circular cylinder. They determined that there is a critical mass ratio 3% below which the NES is ineffective. When the mass ratio was set between 3 and 6%, the results showed multiple solutions and a strong dependence on the initial conditions such as gust, which eliminates its effectiveness. As the mass ratio was increased to 10%, the vibrations were significantly reduced. However, this reduction may be more due to the change in the density ratio of the combined cylinder and NES masses to the density of the surrounding fluid, which affects the lock-in region of the vortex-induced vibrations. They also determined that placing the secondary mass within the main cylinder may be impractical.

The above studies and notions about the response of systems controlled by an NES show that there is a need for careful examination of the response of aeroelastic systems including aircraft wings when combined with a nonlinear energy sink. This is especially true because the payload increase in terms of the mass of the NES and its placement along the chord must be carefully considered. Furthermore, gust effects could cause a change in the initial conditions and unexpected or undesirable responses. The introduction of the NES, which is essentially a cubic nonlinearity to the aeroelastic system, could lead to multiple stable responses depending on such conditions. The objective of this work is to assess the effectiveness of the NES in controlling the flutter and ensuing limit cycle oscillations of a two-dimensional aeroelastic system. Particular attention is placed on its effects on the flutter delay, type of instability and reduction of the ensuing LCO amplitudes. This will be achieved by investigating the dependence of controlled responses on the placement location along the chord of the NES, its mass and the initial conditions. In the following section, we use the energy approach to derive the governing coupled equations of the airfoil-NES system. The aerodynamics are modeled using the nonlinear quasi-steady aerodynamics. In Sect. 3, we perform a linear analysis to determine the effects of

the NES on the onset of flutter. We use, in Sect. 4, the normal form to analytically determine the nonlinear response characteristics of the coupled system and the effects of combining the sink nonlinearity with the system’s nonlinearities. In Sect. 5, we present and discuss the results for different systems and NES parameters. Finally, we give in Sect. 6 the conclusions and some remarks.

### 2 Aeroelastic model

The aeroelastic system under investigation is composed of a rigid wing supported by torsional and flexural springs, as shown in Fig. 1. This wing is allowed to move with two degrees of freedom: (a) a vertical translational motion referred to as plunge and denoted by  $h$  and (b) a clockwise rotational motion referred to as pitch and denoted by  $\theta$ . The relative displacement of the NES mass with respect to the wing is denoted by  $y_2$ . In Fig. 1, the plunge is considered positive in the downward direction and the pitch is assumed positive in the clockwise direction. The position of the center of gravity, leading and trailing edges, etc. are measured with respect to the elastic axis which is the origin of the translating frame. The parameters  $k_h(h)$ ,  $k_\theta(\theta)$  and  $k_n(y_2)$  are used to respectively represent the stiffness of the plunge, pitch and NES. The pitch and plunge stiffness are assumed to have polynomial forms and given by

$$k_h(h) = k_{h_0} + k_{h_1} h + k_{h_2} h^2$$

$$k_\theta(\theta) = k_{\theta_0} + k_{\theta_1} \theta + k_{\theta_2} \theta^2$$

and the NES stiffness is of the form

$$k_n(y_2) = k_{n_2} y_2^2$$

Next, we use the energy approach to derive the equations of motion governing the coupled wing/NES system. The details of the derivation are given in the ‘‘Appendix’’. Based on this derivation, the following set of ordinary differential equations is obtained:

$$\ddot{h} [m_1 + m_2] + \ddot{\theta} [e m_1 + m_2 d] \cos(\alpha_0 + \theta) + m_2 \ddot{y}_2 - e \dot{\theta}^2 m_1 \sin(\alpha_0 + \theta) - m_2 d \dot{\theta}^2 \sin(\alpha_0 + \theta) + k_{h_0} h + k_{h_1} h^2 + k_{h_2} h^3 + C_h \dot{h} = -L \tag{1}$$

$$\ddot{h} [m_1 e + m_2 d] \cos(\alpha_0 + \theta) + \ddot{y}_2 m_2 d \cos(\alpha_0 + \theta) + \ddot{\theta} [m_1 e^2 + I_{cg} + m_2 d^2]$$

$$+ k_{\theta_0} \theta + k_{\theta_1} \theta^2 + k_{\theta_2} \theta^3 + C_\theta \dot{\theta} = M \tag{2}$$

$$m_2 \ddot{h} + \ddot{\theta} [m_2 d \cos(\alpha_0 + \theta)] + m_2 \ddot{y}_2 - 2 m_2 d \dot{\theta}^2 \sin(\alpha_0 + \theta) + k_{n_2} y_2^3 + C_{y_2} \dot{y}_2 = 0 \tag{3}$$

These equations were derived assuming that  $y_2$  is computed from the mid thickness of the airfoil. However, if we assume that  $y_2$  is computed from a fixed point (i.e. the origin of the frame), the following equations are obtained

$$m_1 \ddot{h} + e \ddot{\theta} m_1 \cos(\theta) + k_{h_0} h + k_{h_1} h^2 + k_{h_2} h^3 - k_n (-y_2 - d \sin \theta + h)^3 + C_h \dot{h} - C_{y_2} (\dot{y}_2 + d \dot{\theta} \cos \theta - \dot{h}) = -L \tag{4}$$

$$(I_{cg} + m_1 e^2) \ddot{\theta} + m_1 e \ddot{h} \cos(\theta) + m_2 d^2 \ddot{\theta} + k_{\theta_0} \theta + k_{\theta_1} \theta^2 + k_{\theta_2} \theta^3 - k_n d \cos \theta (-y_2 - d \sin \theta + h)^3 + C_\theta \dot{\theta} + C_{y_2} d \cos \theta (\dot{y}_2 + d \dot{\theta} \cos \theta - \dot{h}) = M \tag{5}$$

$$m_2 \ddot{y}_2 + k_n (y_2 + d \sin \theta - h)^3 + C_{y_2} (\dot{y}_2 + d \dot{\theta} \cos \theta - \dot{h}) = 0 \tag{6}$$

When non-dimensionalized, these equations yield:

$$h'' + e^* \theta'' \cos(\theta) + \frac{\sigma^2}{V^2} (h + \eta_1^h h^2 + \eta_2^h h^3) + \bar{\eta} \frac{\sigma^2}{V^2} (-y_2 - d^* \sin \theta + h)^3 + \frac{\bar{C}_1}{V} h' + \frac{\bar{C}_{y_2} \sigma}{V} (y_2' + d^* \theta' \cos \theta - h') = -\bar{L} \tag{7}$$

$$r^2 \theta'' + e^* \cos(\theta) h'' + \bar{e} d^* \theta'' + \frac{r^2}{V^2} (\theta + \eta_1^\theta \theta^2 + \eta_2^\theta \theta^3) - \bar{\eta} \frac{\sigma^2}{V^2} d^* \cos \theta (-y_2 - d \sin \theta + h)^3 \frac{\bar{C}_2}{V} \theta' + \frac{\bar{C}_{y_2} \sigma}{V} d^* \cos \theta (y_2' + d^* \theta' \cos \theta - h') = \bar{M} \tag{8}$$

$$\bar{e} y_2'' + \bar{\eta} \frac{\sigma^2}{V^2} (y_2 + d^* \sin \theta - h)^3 + \frac{\bar{C}_{y_2} \sigma}{V} (y_2' + d^* \theta' \cos \theta - h') = 0 \tag{9}$$

where  $\bar{e}$  is the mass ratio of the NES relative to the total mass of the system,  $\sigma$  is the frequency ratio,  $V$  is the reduced velocity,  $d$  is the nondimensional location of the NES with respect to the elastic axis,  $\bar{\eta}$  is the nondimensional stiffness associated with the NES,  $e^*$  is the eccentricity,  $\eta_{i=1,2}^h$  are the quadratic and cubic plunging stiffness,  $\eta_{i=1,2}^\theta$  are the quadratic and cubic

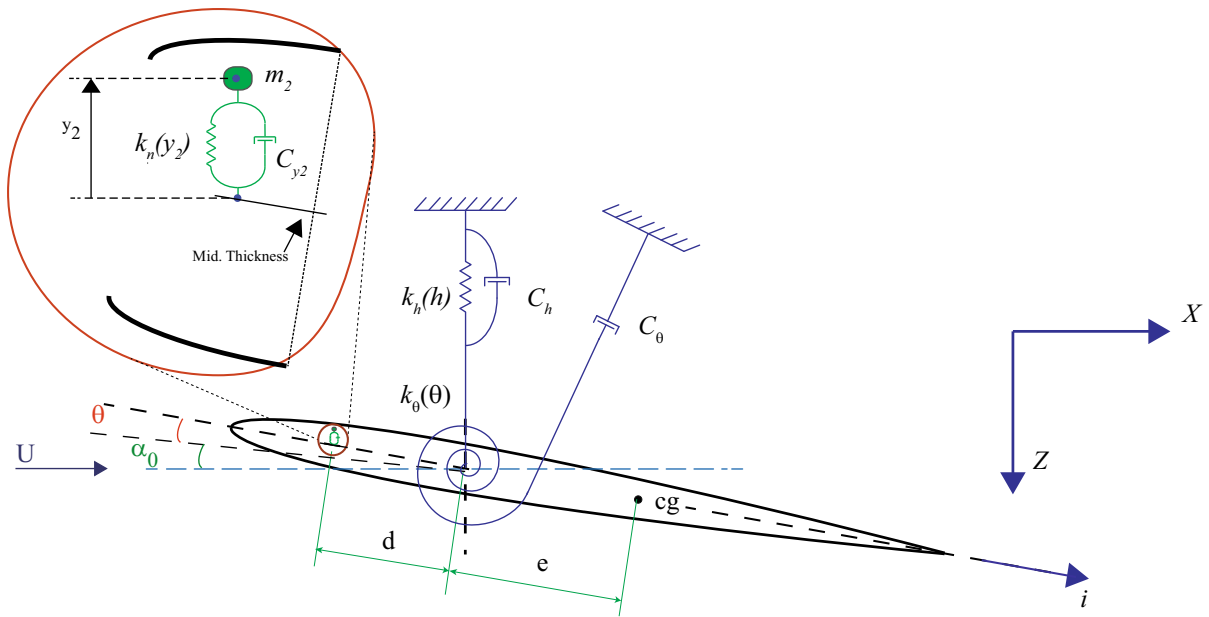


**Fig. 1** Schematic of the airfoil-NES system

pitching stiffness,  $\bar{L}$  is the nondimensional lift and  $\bar{M}$  is the nondimensional moment.

Figure 2 shows a comparison of the amplitudes of the limit cycle oscillations obtained using the models of Lee et al. [1] and Guo et al. [5] and the current model for an NES mass ratio of 5%. The observed differences in the amplitude values are due to the different assumptions made regarding the representation of the aerodynamic forces and moments. In the current work, we use a nonlinear quasi-steady representation. Lee et al. used a linear quasi-steady aerodynamic model while Guo et al used the aerodynamic formulation of Fung et al. [6]. This difference along with the difference in the approximations of the  $\cos \theta$  and  $\sin \theta$  terms and the solution approach yield the observed differences in the LCO amplitudes. Still, the common observation from the three models is that the effect of the NES on delaying flutter is negligible.

In the rest of the work, we make use of Eqs. (1), (2) and (3), assume zero preset angle of attack  $\alpha_0$  (i.e.  $\alpha_0 = 0$ ) and a small pitch angle ( $\theta$ ) to obtain

$$\begin{aligned} \ddot{h} [m_1 + m_2] + \ddot{\theta} \left(1 - \frac{\theta^2}{2}\right) [e m_1 + m_2 d] \\ + m_2 \ddot{y}_2 - e \dot{\theta}^2 m_1 \theta - m_2 d \dot{\theta}^2 \theta + k_{h_0} h + k_{h_1} h^2 \\ + k_{h_2} h^3 + C_h \dot{h} = -L \end{aligned} \tag{10}$$

$$\begin{aligned} \ddot{h} \left(1 - \frac{\theta^2}{2}\right) [m_1 e + m_2 d] + \ddot{y}_2 m_2 d \left(1 - \frac{\theta^2}{2}\right) \\ + \ddot{\theta} [m_1 e^2 + I_{cg} + m_2 d^2] \\ + k_{\theta_0} \theta + k_{\theta_1} \theta^2 + k_{\theta_2} \theta^3 + C_\theta \dot{\theta} = M \end{aligned} \tag{11}$$

$$\begin{aligned} m_2 \ddot{h} + \ddot{\theta} \left(1 - \frac{\theta^2}{2}\right) [m_2 d] + m_2 \ddot{y}_2 - 2 m_2 d \dot{\theta}^2 \theta \\ + k_{n_2} y_2^3 + C_{y_2} \dot{y}_2 = 0 \end{aligned} \tag{12}$$

To model the limit cycle oscillations, one needs to account for the aerodynamic nonlinearities resulting from flow separation, which depends on the effective angle of attack. For accurate evaluation of the nonlinear effects, one would need to solve the Navier-Stokes equations and couple them with the equations of motion of the nonlinear energy sink and airfoil section. Still, such a high-fidelity approach would need to be validated and is computationally expensive. More importantly, it would be impossible to pinpoint underlying physics from such simulations that have a large number of degrees of freedom. As such, we opted for using a reduced-order model of the aerodynamic loads that would allow for the evaluation of the underlying stability and effects of different parameters of the NES, which is the objective of this work. Reduced-order models have their own shortcomings. For instance,

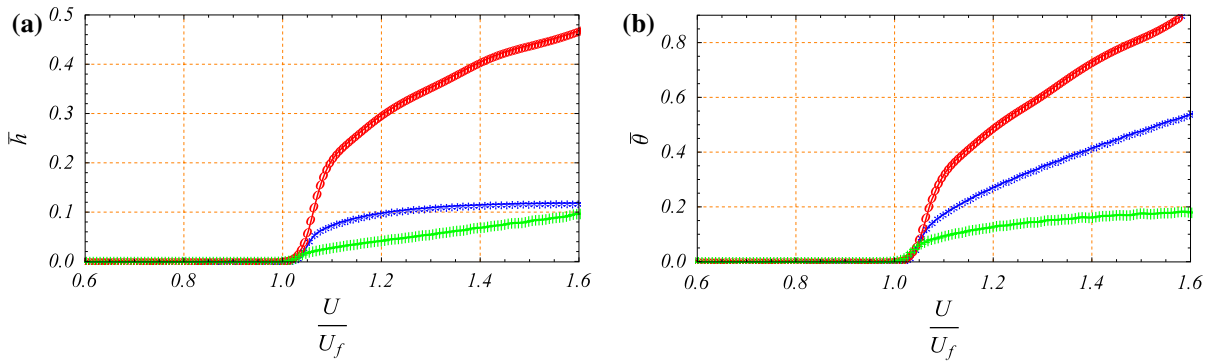


**Fig. 2** Comparison of the results of Lee et al. [1] (—○—), Guo et al. [5] (—\*—) and the current model (—+—) for the **a** plunge and **b** pitch response

unsteady aerodynamic models are mostly linear and are, thus, limited to small angles of attack, which may limit their applicability to the problem considered in this study. As such, we model the aerodynamic loads by a nonlinear quasi-steady approximation [7,8], where the lift and moment are given by:

$$\begin{aligned}
 L &= \rho U^2 b C_{l\alpha} (\alpha_{\text{eff}} - c_s \alpha_{\text{eff}}^3) \\
 M &= \rho U^2 b^2 C_{m\alpha} (\alpha_{\text{eff}} - c_s \alpha_{\text{eff}}^3)
 \end{aligned}
 \tag{13}$$

where  $c_s$  is the nonlinear aerodynamic coefficient,  $C_{l\alpha} = 2\pi$  is the lift coefficient,  $C_{m\alpha} = (\frac{1}{2} + a) C_{l\alpha}$  is the moment coefficient, and  $\alpha_{\text{eff}} = \theta + \frac{\dot{h}}{U} + (\frac{1}{2} - a) \frac{b}{U} \dot{\theta}$  is the effective angle of attack.

### 3 Linear analysis

To study the effects of the NES parameters on the onset of flutter, we eliminate all nonlinear terms of the equations, which yields

$$\begin{aligned}
 &\overbrace{\begin{pmatrix} m_1 + m_2 & m_1 e + m_2 d & m_2 \\ m_1 e + m_2 d & m_1 e^2 + I_{cg} + m_2 d^2 & m_2 d \\ m_2 & m_2 d & m_2 \end{pmatrix}}^{M_{\text{mat}}} \begin{pmatrix} \ddot{h} \\ \ddot{\theta} \\ \ddot{y}_2 \end{pmatrix} \\
 &+ \underbrace{\begin{pmatrix} k_{h0} & 0 & 0 \\ 0 & k_{\theta 0} & 0 \\ 0 & 0 & 0 \end{pmatrix}}^{K_{\text{mat}}} \begin{pmatrix} h \\ \theta \\ y_2 \end{pmatrix}
 \end{aligned}$$

$$\begin{aligned}
 &+ \underbrace{\begin{pmatrix} C_h & 0 & 0 \\ 0 & C_\theta & 0 \\ 0 & 0 & C_{y_2} \end{pmatrix}}_{C_{\text{mat}}} \begin{pmatrix} \dot{h} \\ \dot{\theta} \\ \dot{y}_2 \end{pmatrix} = \underbrace{\begin{pmatrix} 0 & \rho U^2 b C_{l\alpha} & 0 \\ 0 & \rho U^2 b^2 C_{m\alpha} & 0 \\ 0 & 0 & 0 \end{pmatrix}}_{K_{\text{mat}}^a} \begin{pmatrix} h \\ \theta \\ y_2 \end{pmatrix} \\
 &+ \underbrace{\begin{pmatrix} \rho U b C_{l\alpha} & \rho U b^2 C_{l\alpha} (\frac{1}{2} - a) & 0 \\ \rho U b^2 C_{m\alpha} & \rho U b^3 C_{m\alpha} (\frac{1}{2} - a) & 0 \\ 0 & 0 & 0 \end{pmatrix}}_{C_{\text{mat}}^a} \begin{pmatrix} \dot{h} \\ \dot{\theta} \\ \dot{y}_2 \end{pmatrix}
 \end{aligned}
 \tag{14}$$

Using the state variable

$$Y = (h \ \theta \ y_2 \ \dot{h} \ \dot{\theta} \ \dot{y}_2)^T
 \tag{15}$$

we rewrite Eq. (14) as

$$\dot{Y} = B(U) Y
 \tag{16}$$

where

$$B(U) = \begin{pmatrix} 0_{3 \times 3} & I_{3 \times 3} \\ -M_{\text{mat}}^{-1} \times (K_{\text{mat}} - K_{\text{mat}}^a) & -M_{\text{mat}}^{-1} \times (C_{\text{mat}} - C_{\text{mat}}^a) \end{pmatrix}
 \tag{17}$$

Figure 3 shows the variations of the real and imaginary parts of the eigenvalues of the aeroelastic system, having the parameters presented in Table 1, as the freestream velocity  $U$  is increased. The plot shows that the flutter speed is  $18.16 \frac{m}{s}$ .

To investigate further the behavior of the system when the NES is attached, we conduct various simulations. Figures 4a–c, show the effects of the mass  $m_2$  and location of the NES relative to the elastic axis of the airfoil, as defined by the parameter  $d$  in semi-chords on the flutter speed, for damping coefficients

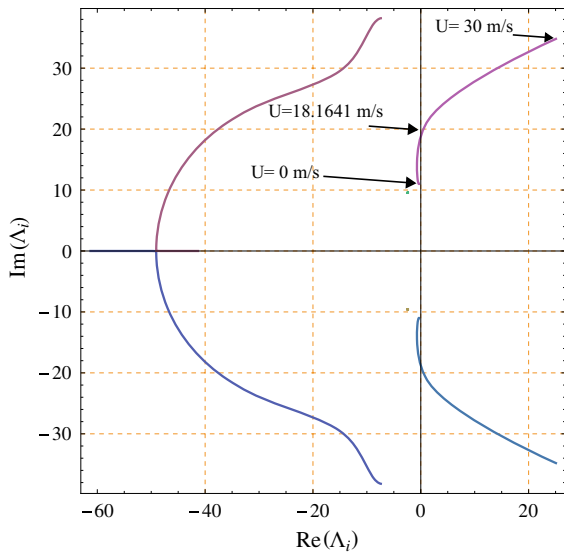


**Fig. 3** Variation of the eigenvalues of the aeroelastic system for  $U \in [0, 30 \frac{m}{s}]$

**Table 1** Numerical parameters of the aeroelastic system

	Considered values	Unit
$m_1$	2.049	kg
$\rho$	1.225	$\frac{kg}{m^3}$
$b$	0.135	m
$I_e$	0.0558	$kg\ m^2$
$k_{\theta_0}$	6.833	N
$k_{h_0}$	2844.4	$\frac{N}{m}$
$k_{\theta_1}$	0	N
$k_{h_1}$	0	$\frac{N}{m^2}$
$C_\theta$	0.036	$\frac{Ns}{m}$
$C_h$	27.43	$\frac{Ns}{m}$
$a$	-0.6847	
$x_\theta$	0.0447	

$C_{y_2} = 0.01, 0.1$  and  $1 \frac{Ns}{m}$ , respectively. It is noted that all of these parameters affect the onset of the flutter. Although increasing the mass causes a small delay in the flutter speed when the NES is placed in front of the elastic axis, the increased mass actually causes the flutter to take place at a lower speed when the NES is placed behind the elastic axis. However, a general observation is that the impact of the NES on the flutter speed is negligible.

### 4 Nonlinear analysis: normal form of the Hopf bifurcation

To determine the effects of the different nonlinear terms on the type of instability, the energy exchange between the wing and the NES and the amplitude of the limit cycle oscillations, we derive the normal form of the Hopf bifurcation [9] of the coupled airfoil-NES system near  $U_f$ . For this purpose, we add a perturbation term  $\epsilon^2 \sigma_U U_f$  to  $U_f$  and seek a first order solution of the form:

$$X = \epsilon X_1 + \epsilon^2 X_2 + \epsilon^3 X_3 \tag{18}$$

where  $\sigma_U$  is a variable small positive number and  $X$  stands for any of the outputs of the system (i.e.  $X = h, \theta$  or  $y_2$ ). We also rewrite the time derivative as:

$$\frac{d}{dt} = \frac{\partial}{\partial \tau_0} + \epsilon^2 \frac{\partial}{\partial \tau_2} = D_0 + \epsilon^2 D_2 \tag{19}$$

where  $\tau_n = \epsilon^n t$ .

Next, we introduce the matrix  $F$  whose columns are the eigenvectors of  $B(U_f)$ , the corresponding eigenvalues are  $\pm j \omega_1 - \mu_1, \pm j \omega_2, -\mu_2$  and 0. Then, we define the vector  $V$  such that  $Y = F V$ . Under these assumptions, and using the state variable  $Y$  defined in Eq. (15), Eqs. (10), (11), (12) and (13) lead to a set of three nonlinear coupled ordinary differential equations defined by the order of  $\epsilon$ , namely  $\epsilon, \epsilon^2$  and  $\epsilon^3$  and written as:

Order ( $\epsilon$ )

$$D_0 V_1 = J_U V_1 \tag{20}$$

Order ( $\epsilon^2$ )

$$D_0 V_2 = J_U V_2 + Q^{\epsilon^2}(V_1, V_1) \tag{21}$$

Order ( $\epsilon^3$ )

$$D_0 V_3 = -D_2 V_1 + J_U V_3 + \sigma_U R V_1 + C^a(V_1, V_1, V_1) + C^b(D_0 V_1, V_1, V_1) \tag{22}$$

where  $J_U = F^{-1} B(U_f) F$  is a diagonal matrix whose elements are the eigenvalues of  $B(U_f)$  namely :  $\pm j \omega_1 - \mu_1, \pm j \omega_2, -\mu_2$  and 0,  $R = F^{-1} B_1(U_f) F$ . We note that  $V_i(2) = \overline{V_i(1)}$  and  $V_i(4) = \overline{V_i(3)}$  (where

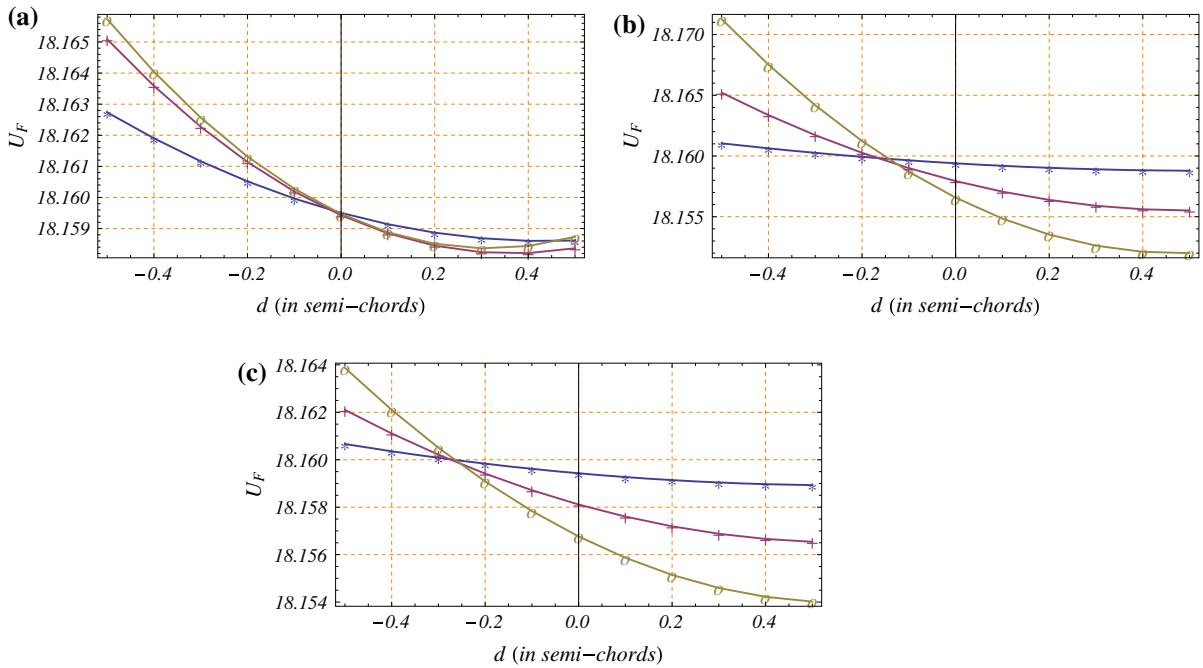


**Fig. 4** Effect of the mass ratio  $\frac{m_2}{m_1}$ , 1%(-\*-), 3%(-+-), 5%(-o-) and location of the NES, on the flutter speed of the airfoil-NES system for **a**  $C_{y2} = 0.01$ , **b**  $C_{y2} = 0.1$  and **c**  $C_{y2} = 1$

$i = 1, 2, 3$  and  $V_i(j)$  is the  $j$ th component of the vector  $V_i$ ; the homogenous solution of  $V_i(1)$  and  $V_i(5)$  are decaying solutions. Consequently, Eqs. (20), (21) and (22) are simplified to

Order ( $\epsilon$ )

$$\begin{aligned} D_0 v_{13} - j \omega_2 v_{13} &= 0 \\ D_0 v_{16} &= 0 \end{aligned} \tag{23}$$

Order ( $\epsilon^2$ )

$$\begin{aligned} D_0 v_{23} - j \omega_2 v_{23} &= \hat{Q}_3^{\epsilon^2}(v_{13}, v_{13}) \\ D_0 v_{26} &= \hat{Q}_6^{\epsilon^2}(v_{16}, v_{16}) \end{aligned} \tag{24}$$

Order ( $\epsilon^3$ )

$$\begin{aligned} D_0 v_{33} - j \omega_2 v_{33} &= -D_2 v_{13} + \sigma_U R v_1 \\ &+ \hat{Q}_3^{\epsilon^3}(v_{13}, v_{23}) + \hat{C}_3^a(v_{13}, v_{13}, \bar{v}_{13}) \\ &+ \hat{C}_3^b(D_0 v_{13}, v_{13}, \bar{v}_{13}) + cc + NST \\ D_0 v_{36} &= -D_2 v_{16} + \sigma_U R v_1 + \hat{Q}_6^{\epsilon^3}(v_{16}, v_{26}) \\ &+ \hat{C}_6^c(v_{16}, v_{16}, \bar{v}_{16}) \end{aligned}$$

$$+ \hat{C}_6^d(D_0 v_{16}, v_{16}, \bar{v}_{16}) + cc + NST \tag{25}$$

where  $v_{ij} = V_i(j)$ ,  $\hat{Q}_3^i(v, v)$  and  $C_3^{a,b,c,d}(v, v, v)$  are bilinear and trilinear functions of  $v$ , respectively and where  $NST$  stands for nonsecular terms and  $cc$  stands for complex conjugate of the preceding terms in the equation. The solution of Eq. (23) is given by:

$$\begin{aligned} v_{13}(\tau_0) &= G(T_2)e^{j\omega_2 \tau_0} \\ v_{16}(\tau_0) &= H(T_2) \end{aligned} \tag{26}$$

where  $G$  denotes the complex amplitudes of the pitch and plunging motions of the airfoil section and  $H$  denotes the amplitude of the NES oscillations. Substituting Eqs. (26) into (24) and solving for the particular solution, we obtain:

$$\begin{aligned} v_{23} &= e^{j\omega_2 \tau_0} \int e^{-j\omega_2 x} \hat{Q}_3^{\epsilon^2}(v_{13}(x), v_{13}(x)) dx \\ v_{26} &= \hat{Q}_6^{\epsilon^2}(v_{16}, v_{16}) \tau_0 \end{aligned} \tag{27}$$

Substituting Eqs. (27) into (25) and removing the secular terms, the complex-valued normal form of the Hopf bifurcation is obtained as



$$D_2 G = \eta G + \phi_e G^2 \bar{G} + \gamma H^2 G \tag{28}$$

$$D_2 H = \kappa G \bar{G} H + \lambda H^3 \tag{29}$$

The complex coefficient  $\eta$  represents the growth rate and frequency of the oscillations of the airfoil section. The effective nonlinearity  $\phi_e$  denotes the role of the different system’s nonlinearities in limiting the amplitude of the motion of the airfoil section.  $H$  is a real number and, as such,  $\lambda$  is directly related to the nonlinear stiffness of the energy sink. The parameters  $\gamma$  and  $\kappa$  are related to the energy exchange between the airfoil section and the nonlinear energy sink.

By letting  $G(T_2) = \frac{1}{2} w e^{i\zeta(T_2)}$  and separating the real and imaginary parts of Eqs. (28) and (29), we obtain the following real-valued normal form of the Hopf bifurcation:

$$w' = \eta_r w + \frac{1}{4} \phi_{er} w^3 + \frac{1}{2} \gamma_r H^2 w \tag{30}$$

$$\zeta' = \eta_i + \frac{1}{4} \phi_{ei} w^2 + \gamma_i H^2 \tag{31}$$

$$H' = \frac{1}{4} \kappa_r w^2 H + \frac{1}{4} \lambda_r H^3 \tag{32}$$

$$0 = \frac{1}{4} \kappa_i w^2 + \lambda_i H^2 \tag{33}$$

where  $w$  is the amplitude of oscillations and  $\zeta$  is the shifting angle whose time variation is related to the frequency of the oscillations. The signs of  $\eta_r$  and  $\phi_{er}$  determine the type of bifurcation Nayfeh et al. [10]. A supercritical Hopf bifurcation is obtained for  $\eta_r > 0$  and  $\phi_{er} > 0$  and a subcritical Hopf bifurcation is obtained for  $\eta_r < 0$  and  $\phi_{er} > 0$ . The two parameters,  $\gamma_r$  and  $\kappa_r$  are of particular importance to the current problem because they represent the rate of energy exchange between the airfoil section and the nonlinear sink. As expected, both of these parameters would depend on the nonlinear stiffness of the energy sink with a coefficient that depends on the mass ratio and the amplitude of the limit cycle oscillations.

### 5 Results and discussion

We consider the effects of a nonlinear energy sink on a wing section having the parameters shown in Table 1. For this wing the expression of the effective nonlinearity and growth rate without NES are given by

$$\eta_r = 0.433987 \sigma_U U_f$$

$$\phi_{er} = 0.0000213689 - 0.00657702 cs$$

$$\begin{aligned} & - 1.24153 \times 10^{-15} k_{h1}^2 - 1.68515 \times 10^{-10} k_{h2} \\ & - 7.14763 \times 10^{-10} k_{h1} k_{\theta_1} \\ & - 0.0000171762 k_{\theta_1}^2 + 0.000213956 k_{\theta_2} \end{aligned} \tag{34}$$

As explained above, the signs of  $\eta_r$  and  $\phi_{er}$  determine whether the instability is supercritical or subcritical. We note that the cubic pitch nonlinearity  $k_{\theta_2}$  contributes to a subcritical Hopf bifurcation since it contributes to a positive  $\phi_{er}$ . However, the pitch quadratic nonlinearity,  $k_{\theta_1}$ , as well as the cubic aerodynamic nonlinearity,  $c_s$ , have a negative contribution to  $\eta_r$  which lead to a supercritical instability.

Next we add a nonlinear energy sink to the airfoil section. Two different cases of mass ratios, namely, 5 and 3% are considered. For each of these cases, three cases for the location of the sink along the chord are considered. These include placing the sink at the elastic axis,  $d = 0$ , ahead of the elastic axis,  $d = -0.3 b$ , and behind the elastic axis,  $d = 0.3 b$ . The growth rates of the amplitudes of the oscillations for these cases are  $\eta_r = 0.267653 \times \sigma_U U_f$  for  $d = 0$ ,  $\eta_r = 0.272251 \times \sigma_U U_f$ , for  $d = -0.3 b$  and  $\eta_r = 0.265612 \times \sigma_U U_f$ , for  $d = 0.3 b$ .

#### 5.1 Case of 5% mass ratio

The coefficients of the effective nonlinearity of the system and the other terms of the normal form as derived above for an NES mass of 5% are given by

$$\begin{aligned} \phi_{er} &= -0.00157815 - 0.0181067 cs - 7.94452 \\ & \times 10^{-12} k_{h1}^2 - 1.59542 \times 10^{-7} k_{h2} \\ & - 3.86976 \times 10^{-7} k_{n2} - 5.2063 \times 10^{-8} k_{h1} k_{\theta_1} \\ & - 0.0000218303 k_{\theta_1}^2 + 0.000502663 k_{\theta_2} \\ \gamma_r &= -0.00476769 k_{n2} \\ \kappa_r &= -0.000973996 k_{n2} \\ \lambda_r &= -2 k_{n2} \\ \kappa_i &= 0 \\ \lambda_i &= 0 \end{aligned} \tag{35}$$

for  $d = -0.3 b$ ,



$$\begin{aligned}
\phi_{er} &= -0.00154919 - 0.0179625 cs - 7.5623 \\
&\quad \times 10^{-12} k_{h_1}^2 - 1.53456 \times 10^{-7} k_{h_2} \\
&\quad - 7.11105 \times 10^{-8} k_{n_2} - 5.13344 \times 10^{-8} k_{h_1} k_{\theta_1} \\
&\quad - 0.0000216527 k_{\theta_1}^2 + 0.000494614 k_{\theta_2} \\
\gamma_r &= -0.00146539 k_{n_2} \\
\kappa_r &= -0.000582321 k_{n_2} \\
\lambda_r &= -2 k_{n_2} \\
\kappa_i &= 0 \\
\lambda_i &= 0
\end{aligned} \tag{36}$$

for  $d = 0$ , and

$$\begin{aligned}
\phi_{er} &= -0.00154374 - 0.0180555 cs - 7.40378 \\
&\quad \times 10^{-12} k_{h_1}^2 - 1.5157 \times 10^{-7} k_{h_2} \\
&\quad - 8.40011 \times 10^{-9} k_{n_2} - 5.13289 \times 10^{-8} k_{h_1} k_{\theta_1} \\
&\quad - 0.0000216049 k_{\theta_1}^2 + 0.000491564 k_{\theta_2} \\
\gamma_r &= -0.000344654 k_{n_2} \\
\kappa_r &= -0.000292471 k_{n_2} \\
\lambda_r &= -2 k_{n_2} \\
\kappa_i &= 0 \\
\lambda_i &= 0
\end{aligned} \tag{37}$$

for  $d = 0.3 b$

In all cases, the energy sink is helpful in terms of contributing toward a supercritical bifurcation. As for the energy transfer between the airfoil section and the nonlinear sink, we note that the value of  $\gamma_r$  is negative in all cases indicating that the nonlinear energy sink can reduce the growth rate of the oscillations, depending on the value of the nonlinear stiffness of the energy sink and the amplitude of the limit cycle oscillations and the sink's oscillations. It is important to note here that the sink does not contribute to decreasing the amplitude of oscillations unless the system starts to oscillate. Furthermore, this contribution is dependent on the amplitude of the NES itself. So, it does not delay the flutter point. Rather, it can, once the oscillations of the wing and NES have grown, reduce the amplitude of the oscillations. On the other hand, the values of  $\kappa_r$  and  $\lambda_r$  are negative which indicates that the amplitude of the NES is decaying at the same time that it draws energy from the wing. This decay impacts its effectiveness in continuously draw-

ing energy from the wing to act like a sink. The reason is that once the amplitudes go below a specific value, the sink stops drawing energy which results in a recovery of the original amplitudes of the wing oscillations. So, the wing response exhibits modulated rather than controlled characteristics as will be shown below.

## 5.2 Case of 3% mass ratio

The expression of the effective nonlinearity of the system and the other parameters of the normal form when the NES mass is 3% are

$$\begin{aligned}
\phi_{er} &= -0.00156868 - 0.0181215 cs - 7.9393 \\
&\quad \times 10^{-12} k_{h_1}^2 - 1.5957 \times 10^{-7} k_{h_2} \\
&\quad - 4.60049 \times 10^{-7} k_{n_2} - 5.2163 \times 10^{-8} k_{h_1} k_{\theta_1} \\
&\quad - 0.0000218307 k_{\theta_1}^2 + 0.000502073 k_{\theta_2} \\
\gamma_r &= -0.0062891 k_{n_2} \\
\kappa_r &= -0.000877802 k_{n_2} \\
\lambda_r &= -2 k_{n_2} \\
\kappa_i &= 0 \\
\lambda_i &= 0
\end{aligned} \tag{38}$$

for  $d = -0.3 b$ ,

$$\begin{aligned}
\phi_{er} &= -0.00155343 - 0.0180097 cs - 7.6002 \\
&\quad \times 10^{-12} k_{h_1}^2 - 1.53984 \times 10^{-7} k_{h_2} \\
&\quad - 1.81754 \times 10^{-8} k_{n_2} - 5.15074 \times 10^{-8} k_{h_1} k_{\theta_1} \\
&\quad - 0.0000217267 k_{\theta_1}^2 + 0.000496234 k_{\theta_2} \\
\gamma_r &= -0.000416306 k_{n_2} \\
\kappa_r &= -0.000523905 k_{n_2} \\
\lambda_r &= -2 k_{n_2} \\
\kappa_i &= 0 \\
\lambda_i &= 0
\end{aligned} \tag{39}$$

for  $d = 0$ , and

$$\begin{aligned}
 \phi_{er} &= -0.00154457 - 0.0181065 \text{ cs} - 7.46618 \\
 &\quad \times 10^{-12} k_{h_1}^2 - 1.52212 \times 10^{-7} k_{h_2} \\
 &\quad + 4.60067 \times 10^{-8} k_{n_2} - 5.15131 \times 10^{-8} k_{h_1} k_{\theta_1} \\
 &\quad - 0.0000217138 k_{\theta_1}^2 + 0.000494204 k_{\theta_2} \\
 \gamma_r &= 0.00209951 k_{n_2} \\
 \kappa_r &= -0.000262956 k_{n_2} \\
 \lambda_r &= -2 k_{n_2} \\
 \kappa_i &= 0 \\
 \lambda_i &= 0
 \end{aligned}
 \tag{40}$$

for  $d = 0.3 b$

The results of this case, 3%, show similar responses to those of the 5% case except for the case where the NES is placed behind the elastic axis. Under these conditions, the NES contributes to a subcritical response as exhibited by the positive coefficient of  $k_{n_2}$  in Eq. 40. We should also note the positive sign of  $\gamma_r$  in the same equation indicating that the energy can not be transferred to the NES under these conditions.

### 5.3 Case of the original system exhibiting subcritical behavior

In this section, we choose the nonlinear parameters of the system without NES such that a subcritical Hopf bifurcation is obtained (i.e.  $k_{\theta_1} = 9.97 \text{ Nm}$ ,  $k_{\theta_2} = 67.69 \text{ Nm}$  and  $k_{h_1} = k_{h_2} = 0$ ) We present in Fig. 5 the bifurcation diagram for the system when the NES is deactivated. The response is subcritical. which

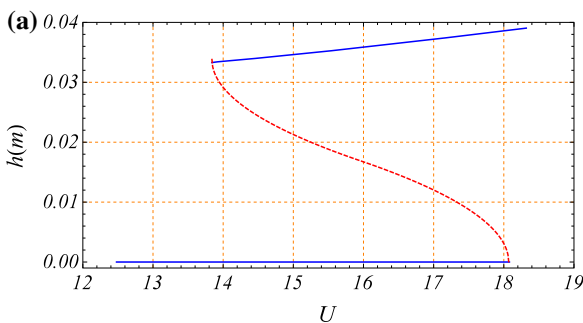


**Table 2** Numerical nonlinear parameters of the NES

	Considered values	Unit
$m_2$	$0.05 \times m_1$	kg
$C_{y_2}$	0.5	$\frac{\text{Ns}}{\text{m}}$
$k_{n_2}$	$1.5 \times 10^5$	$\frac{\text{N}}{\text{m}^3}$
cs	0	

means that a reduction of the freestream velocity does not lead to a decay of the amplitudes of oscillations. This response is dependent on the initial conditions. In fact, for velocities below flutter and for proper initial conditions, the system can exhibit large amplitudes limit cycle oscillations.

Activating the NES, and using the parameters presented in Table 2 we obtain the results plotted in Figs. 6a–c and 7a–c for the cases of  $m_2 = 0.03 m_1$  and  $m_2 = 0.05 m_1$  respectively. The results show that adding the NES changed the subcritical response to a supercritical one over a small region of velocities near flutter. Unlike the subcritical response, the supercritical response is characterized by a progressive increase in the amplitudes of the LCOs as the freestream velocity is increased. The main feature of this response is the recovery, by the airfoil-NES system, of the decaying solution when the freestream velocity is decreased. On the other hand, the numerical solutions shows that although the NES changed the type of instability near the bifurcation point, the system recovered its subcritical property as the speed was increased slightly beyond the initial region of supercritical instability. That is the effect of the NES in changing the type of insta-

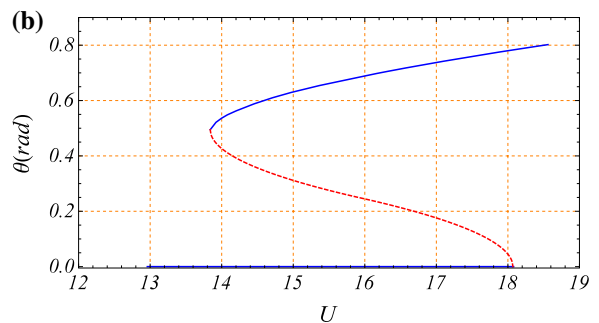


**Fig. 5** Bifurcation diagrams of the **a** plunge and **b** pitch responses for the aeroelastic system having the parameters presented in Table 1 and without NES ( $k_{\theta_1} = 9.967 \text{ Nm}$ ,  $k_{\theta_2} =$

$67.685 \text{ Nm}$ ,). The *continuous lines* represent the stable solution, the *dotted line*, the unstable solution

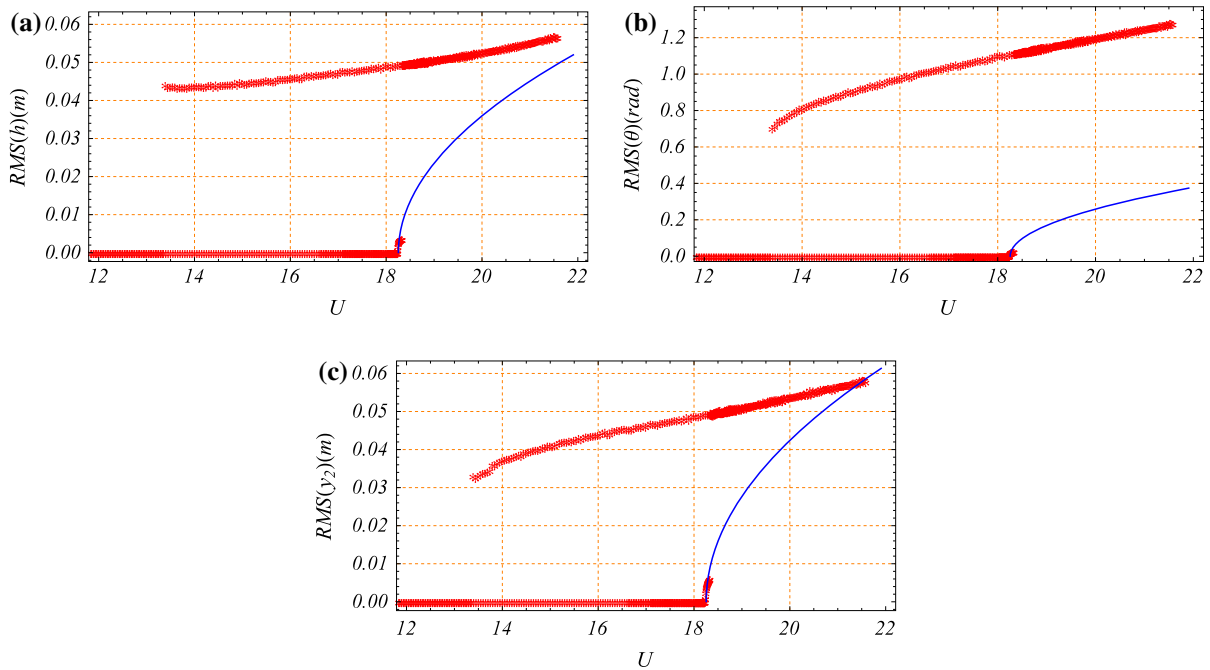


**Fig. 6** Bifurcation diagrams for **a** the plunge, **b** the pitch and **c** NES responses, when the NES is activated in the airfoil-NES system having the parameters presented in Table 1 with  $k_{\theta_1} = 9.967 \text{ Nm}$ ,  $k_{\theta_2} = 67.685 \text{ Nm}$ , and  $k_{n_2} = 150,000 \frac{\text{N}}{\text{m}^2}$ .

The mass of the NES is 3% of the total mass of the wing. The *dots* are numerical simulations and the *solid line* is the normal form (valid only near bifurcation point)

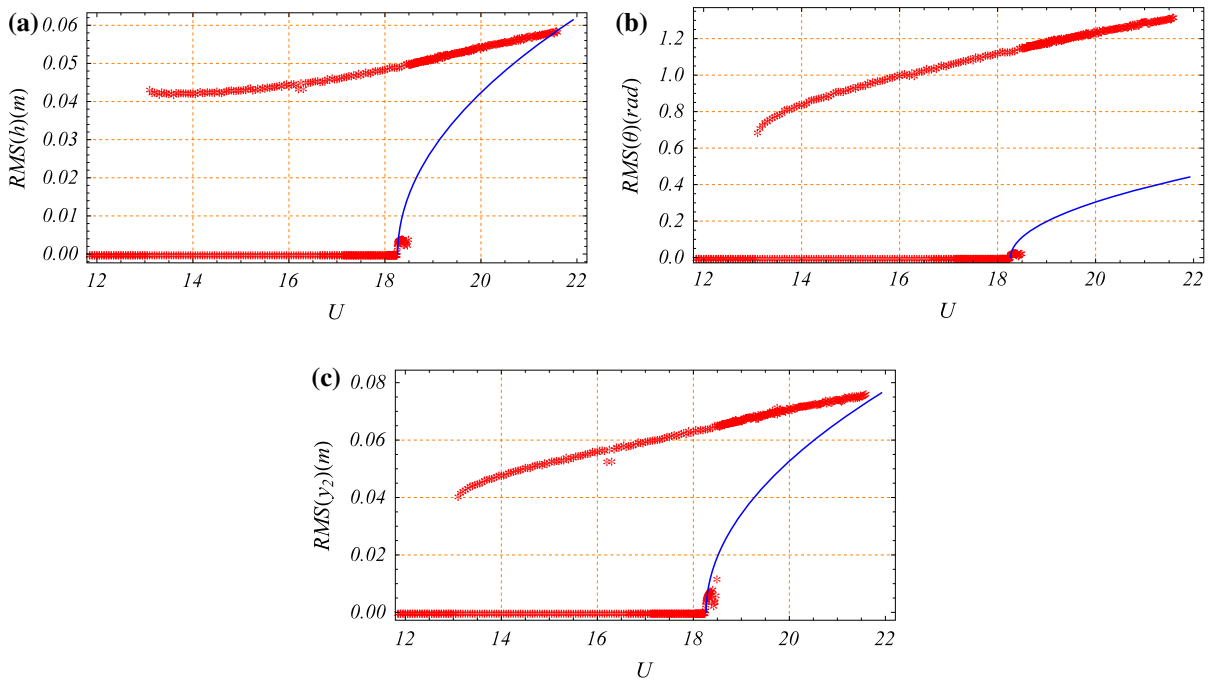
bility was limited to a small region near the flutter speed. We should note here that for the NES mass of  $m_2 = 0.01 m_1$  the type of the Hopf bifurcation remained subcritical. Therefore, the NES with a low mass is ineffective. It is also noted that for the NES to be effective a large value of the nonlinear stiffness  $k_{n_2}$  is needed ( $1.5 \times 10^5$ ).

Figure 8 shows the time series and phase portraits of the plunge, pitch and NES responses at a speed of 18.37 m/s. The plots show a periodic response with one frequency. However, as the speed is slightly increased to 18.43 m/s, we observe a totally different response as shown in Fig. 9. Particularly, as the pitch and plunge amplitudes increase, the amplitude of the NES increases, which indicates that the NES is drawing energy from the motions of the primary system. However, and as shown in the normal form analysis presented above, once enough energy is drawn and the amplitudes of the pitch and plunge oscillations decrease, the NES does not draw any energy from the main oscillations, which results in an increase of the amplitudes of these oscillations of the primary system.

As such, these responses exhibit modulated behaviors as predicted by the analysis presented in Sect. 5.1. It is important to note that the coupled systems responses exhibited different characteristics over the small region between 18.26 and 18.5 m/s.

#### 5.4 Case of the original system exhibiting supercritical behavior

In this section, we consider the case of an aeroelastic system that exhibits a supercritical Hopf bifurcation when the NES is deactivated. The considered parameters are:  $k_{\theta_1} = 90 \text{ Nm}$  and  $k_{\theta_2} = k_{h_2} = k_{h_1} = 0$ . Figure 10 shows the bifurcation diagram for the system without NES. The plots in Figs. 11 and 12 show the bifurcation diagram when the NES is activated for the cases of 3 and 5% respectively. A comparison of the plots in the three figures as presented in Fig. 13 shows that the NES can reduce the amplitude of the wing oscillations as the freestream velocity is increased. However, this reduction is effective over a very small region of increased freestream velocity. Beyond this limited region, the



**Fig. 7** Bifurcation diagrams for **a** the plunge, **b** the pitch and **c** NES responses, when the NES is activated in the airfoil-NES system having the parameters presented in Table 1 with  $k_{\theta_1} = 9.967 \text{ Nm}$ ,  $k_{\theta_2} = 67.685 \text{ Nm}$ , and  $k_{n_2} = 150000 \frac{\text{N}}{\text{m}^2}$ . The

mass of the NES is 5% of the total mass of the wing. The dots are numerical simulations and the solid line is the normal form (valid only near bifurcation point)

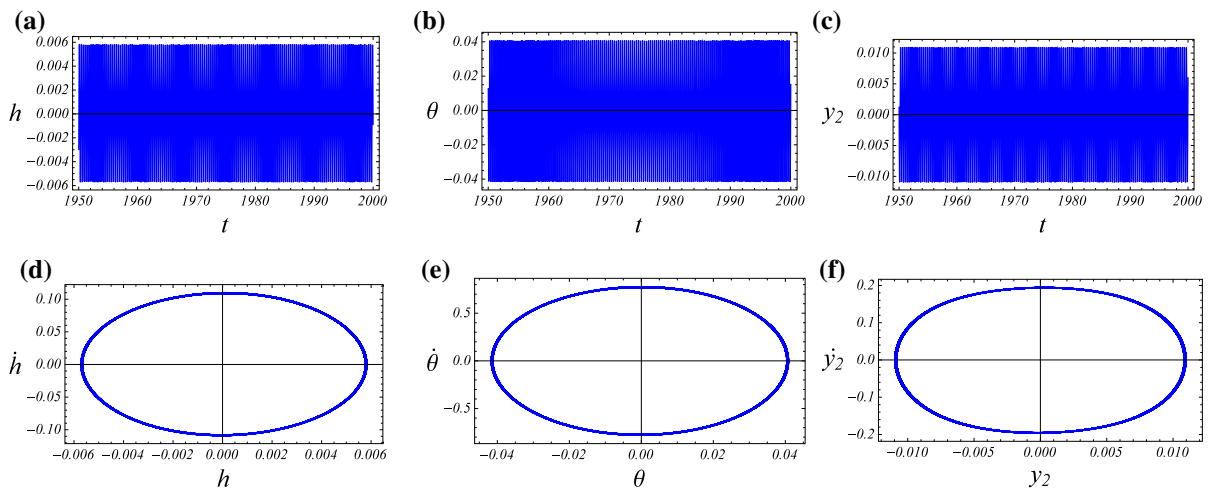


**Fig. 8** Phase portrait and time series for the system with NES mass of 5% when  $U = 18.3861 \text{ m/s}$ ,  $d = -0.3 \times b$  and system parameters of Fig. 7

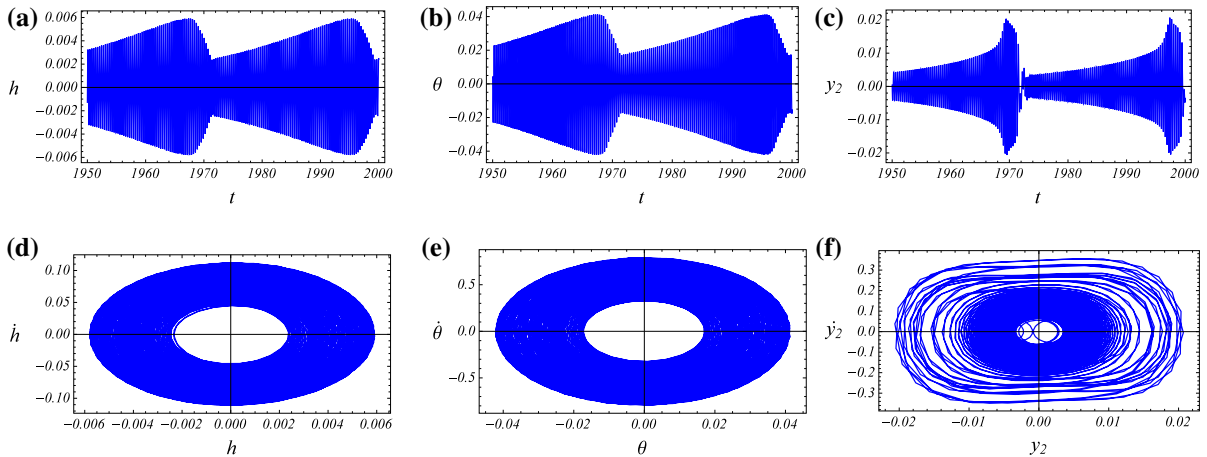


**Fig. 9** Phase portrait and time series for the system with NES mass of 5% when  $U = 18.4261$  m/s,  $d = -0.3 \times b$  and system parameters of Fig. 7

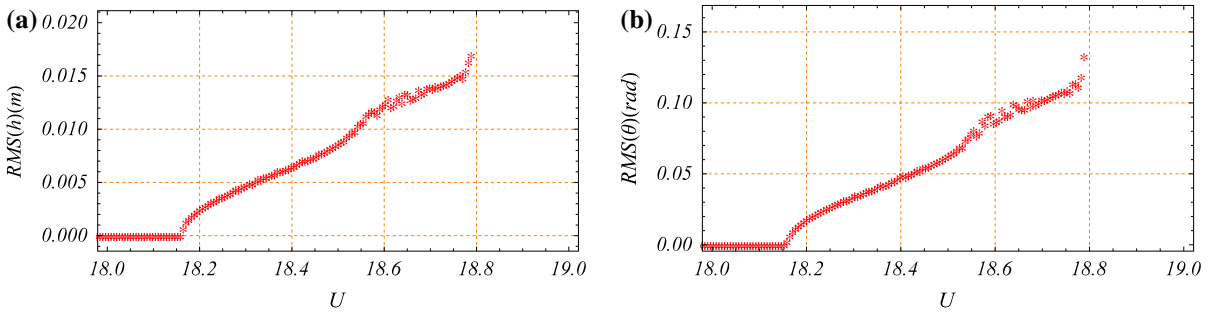


**Fig. 10** Bifurcation diagrams for **a** the plunge, **b** the pitch responses, when the NES is deactivated. The airfoil-NES system parameters are presented in Table 1 with  $k_{\theta_1} = 90$  Nm

wing oscillations recover their original amplitude values indicating the limited region of effectiveness of the NES in terms of reducing the LCO amplitudes of the original system.

**6 Conclusions**

We investigated the effectiveness of using a nonlinear energy sink to passively control the response of a pitching-plunging airfoil section. We used the normal form to quantify the contribution of the sink to the system’s nonlinear response. We used numerical integration to determine the system’s response over a wide range of operating conditions. The results show

that depending on its mass and location along the airfoil, the nonlinear sink can be more effective in terms of changing a subcritical bifurcation to a supercritical one. However, the change is very limited in that the system recovers the subcritical response as the freestream velocity is increased. For the case where the original system exhibits supercritical behavior the results show that the NES can reduce the pitch and plunge amplitudes. However, this reduction is limited to a very small region of freestream velocities above the flutter speed. The results of the normal form show that the nonlinear sink has a decaying characteristics and as such cannot maintain the energy it draws from the airfoil section. This results in modulated responses of both the airfoil section and nonlinear sink.

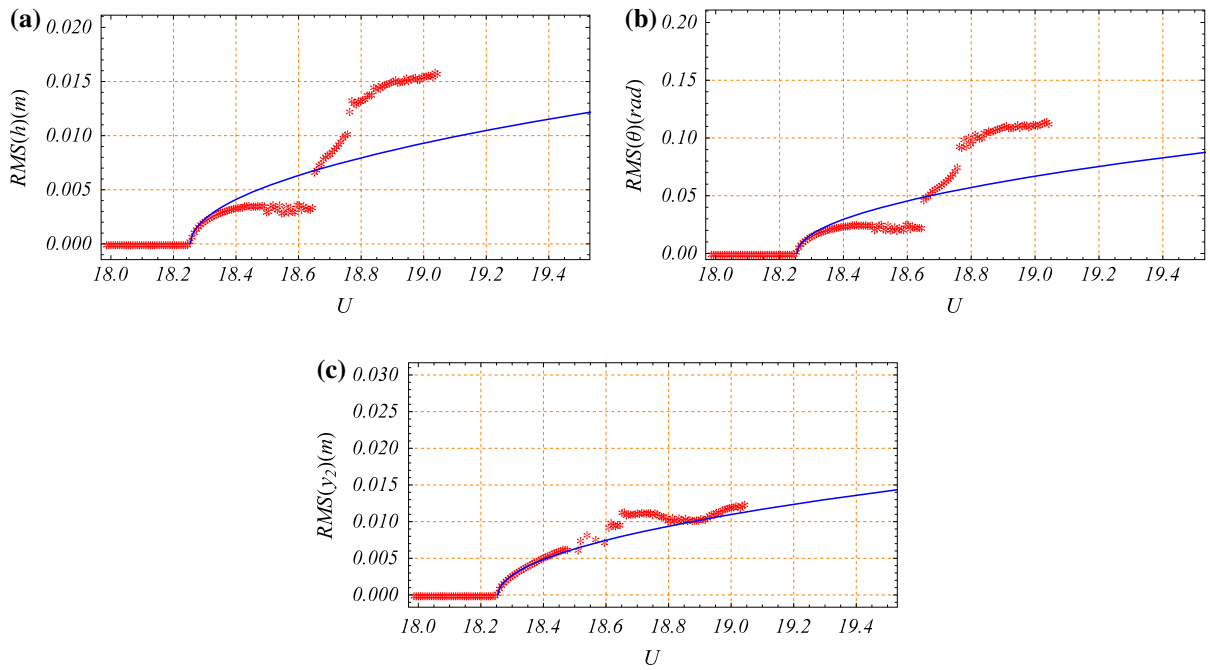


**Fig. 11** Bifurcation diagrams for **a** the plunge, **b** the pitch and **c** NES responses, when the NES is activated. The airfoil-NES system parameters are presented in Table 1 with NES mass of 3%

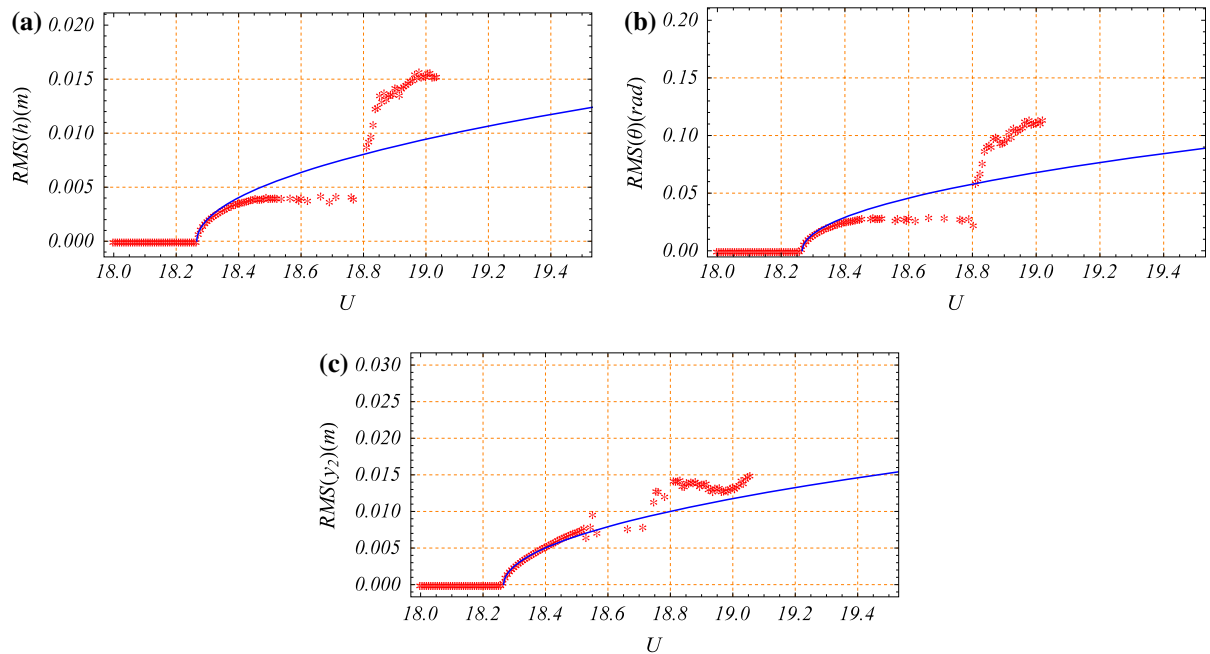


**Fig. 12** Bifurcation diagrams for **a** the plunge, **b** the pitch and **c** NES responses, when the NES is activated. The airfoil-NES system parameters are presented in Table 1 with NES mass of 5%

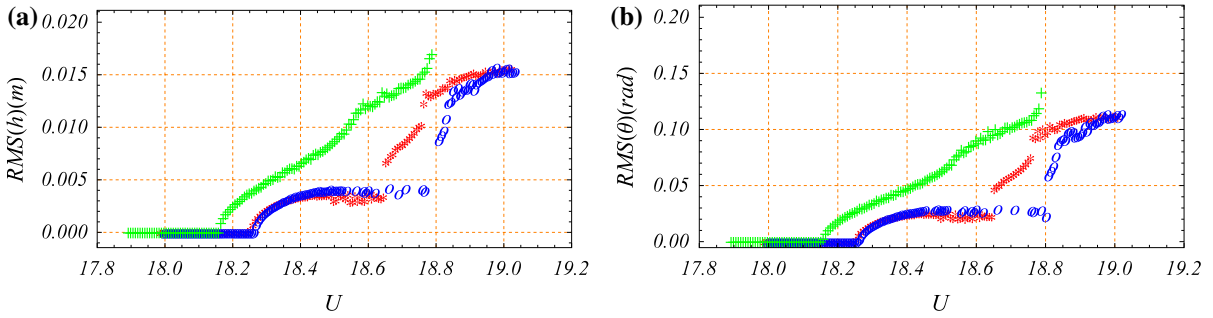


**Fig. 13** Superposition of bifurcation diagrams for **a** the plunge and **b** the pitch, when the NES is de/activated in the airfoil-NES system having the parameters presented in Table 1 with

$k_{\theta_1} = 90$ ,  $k_{\theta_2} = 0$ , and  $k_{n_2} = 150,000$ . The mass of the NES is 0% (+), 3% (\*) and 5% (o) of the total mass of the wing

**Appendix: Derivation of the equations of motion**

Position of the center of gravity of the airfoil:

$$\mathbf{R}_1 = h\mathbf{z} + e\mathbf{i}$$

where  $\mathbf{i} = \cos(\alpha_0 + \theta)\mathbf{x} + \sin(\alpha_0 + \theta)\mathbf{z}$

$$\mathbf{R}_1 = [h + e \sin(\alpha_0 + \theta)]\mathbf{z} + e \cos(\alpha_0 + \theta)\mathbf{x} \tag{41}$$

The velocity then given by

$$\mathbf{V}_1 = [\dot{h} + e\dot{\theta} \cos(\alpha_0 + \theta)]\mathbf{z} - e\dot{\theta} \sin(\alpha_0 + \theta)\mathbf{x} \tag{42}$$

which yields

$$V_1^2 = [\dot{h} + e\dot{\theta} \cos(\alpha_0 + \theta)]^2 + e^2\dot{\theta}^2 \sin^2(\alpha_0 + \theta)$$

$$V_1^2 = \dot{h}^2 + e^2\dot{\theta}^2 \cos^2(\alpha_0 + \theta) + 2e\dot{h}\dot{\theta} \cos(\alpha_0 + \theta) + e^2\dot{\theta}^2 \sin^2(\alpha_0 + \theta)$$

$$V_1^2 = \dot{h}^2 + e^2\dot{\theta}^2 + 2e\dot{h}\dot{\theta} \cos(\alpha_0 + \theta)$$

The position of the NES mass is given by

$$\mathbf{R}_2 = h\mathbf{z} + d\mathbf{i} + y_2\mathbf{z}$$

$$\mathbf{R}_2 = h\mathbf{z} + d \cos(\alpha_0 + \theta)\mathbf{x} + d \sin(\alpha_0 + \theta)\mathbf{z} + y_2\mathbf{z}$$

$$\mathbf{R}_2 = [h + d \sin(\alpha_0 + \theta) + y_2]\mathbf{z} + d \cos(\alpha_0 + \theta)\mathbf{x} \tag{43}$$

its velocity is given by

$$\mathbf{V}_2 = [\dot{h} + d\dot{\theta} \cos(\alpha_0 + \theta) + \dot{y}_2]\mathbf{z} - d\dot{\theta} \sin(\alpha_0 + \theta)\mathbf{x} \tag{44}$$

which yields

$$V_2^2 = (\dot{h} + d\dot{\theta} \cos(\alpha_0 + \theta) + \dot{y}_2)^2 + d^2\dot{\theta}^2 \sin^2(\alpha_0 + \theta)$$

$$V_2^2 = \dot{h}^2 + d^2\dot{\theta}^2 \cos^2(\alpha_0 + \theta) + \dot{y}_2^2 + 2d\dot{h}\dot{\theta} \cos(\alpha_0 + \theta) + 2\dot{h}\dot{y}_2 + 2d\dot{\theta} \cos(\alpha_0 + \theta)\dot{y}_2 + d^2\dot{\theta}^2 \sin^2(\alpha_0 + \theta)$$

$$V_2^2 = \dot{h}^2 + d^2\dot{\theta}^2 + \dot{y}_2^2 + 2d\dot{h}\dot{\theta} \cos(\alpha_0 + \theta) + 2\dot{h}\dot{y}_2 + 2d\dot{\theta} \cos(\alpha_0 + \theta)\dot{y}_2$$

The distance separating  $m_2$  and the elastic axis is given by

$$r^2 = d^2 + y_2^2 + 2dy_2 \sin(\alpha_0 + \theta)$$

The kinetic energy of the system is

$$T = \frac{1}{2}m_1V_1^2 + \frac{1}{2}m_2V_2^2 + \frac{1}{2}I_{cg}\dot{\theta}^2$$

The potential energy of the system



$$PE = \frac{1}{2}k_h h^2 + \frac{1}{2}k_\theta \theta^2 + \frac{1}{2}k_n y_2^2$$

Rayleigh's friction function

$$\mathcal{R} = \frac{1}{2}C_h \dot{h}^2 + \frac{1}{2}C_\theta \dot{\theta}^2 + \frac{1}{2}C_{y_2} \dot{y}_2^2$$

The Lagrange's function

$$\begin{aligned} L &= T - V \\ &= \frac{1}{2}m_1 \left[ \dot{h}^2 + e^2 \dot{\theta}^2 + 2e\dot{h}\dot{\theta} \cos(\alpha_0 + \theta) \right] \\ &\quad + \frac{1}{2}m_2 \left[ \dot{h}^2 + d^2 \dot{\theta}^2 + \dot{y}_2^2 + 2d\dot{h}\dot{\theta} \cos(\alpha_0 + \theta) \right. \\ &\quad \left. + 2\dot{h}\dot{y}_2 + 2d\dot{\theta}\dot{y}_2 \cos(\alpha_0 + \theta) \right] \\ &\quad + \frac{1}{2}I_{cg} \dot{\theta}^2 - \frac{1}{2}k_h h^2 - \frac{1}{2}k_\theta \theta^2 - \frac{1}{2}k_n y_2^2 \\ \frac{\partial L}{\partial \dot{h}} &= \frac{1}{2}m_1 [2\dot{h} + 2e\dot{\theta} \cos(\alpha_0 + \theta)] \\ &\quad + \frac{1}{2}m_2 [2\dot{h} + 2d\dot{\theta} \cos(\alpha_0 + \theta) + 2\dot{y}_2] \end{aligned}$$

thus:

$$\begin{aligned} \frac{\partial L}{\partial \dot{h}} &= m_1 \dot{h} + e\dot{\theta} m_1 \cos(\alpha_0 + \theta) + m_2 \dot{h} \\ &\quad + m_2 d\dot{\theta} \cos(\alpha_0 + \theta) + m_2 \dot{y}_2 \end{aligned}$$

$$\begin{aligned} \frac{\partial L}{\partial \dot{\theta}} &= \frac{1}{2}m_1 [2e^2 \dot{\theta} + 2e\dot{h} \cos(\alpha_0 + \theta)] \\ &\quad + \frac{1}{2}m_2 [2d^2 \dot{\theta} + 2d\dot{h} \cos(\alpha_0 + \theta) \\ &\quad + 2d\dot{y}_2 \cos(\alpha_0 + \theta)] + I_{cg} \dot{\theta} \end{aligned}$$

$$\begin{aligned} \frac{\partial L}{\partial \dot{\theta}} &= m_1 e^2 \dot{\theta} + m_1 e \dot{h} \cos(\alpha_0 + \theta) \\ &\quad + m_2 d^2 \dot{\theta} + m_2 d \dot{h} \cos(\alpha_0 + \theta) \\ &\quad + m_2 d \dot{y}_2 \cos(\alpha_0 + \theta) + I_{cg} \dot{\theta} \end{aligned}$$

$$\frac{\partial L}{\partial \dot{y}_2} = \frac{1}{2}m_2 [2\dot{y}_2 + 2\dot{h} + 2d\dot{\theta} \cos(\alpha_0 + \theta)]$$

$$\frac{\partial L}{\partial \dot{y}_2} = m_2 \dot{y}_2 + m_2 \dot{h} + m_2 d \dot{\theta} \cos(\alpha_0 + \theta)$$

$$\frac{\partial L}{\partial h} = -k_h h$$

$$\begin{aligned} \frac{\partial L}{\partial \theta} &= \frac{1}{2}m_1 [-2e\dot{h}\dot{\theta} \sin(\alpha_0 + \theta)] \\ &\quad + \frac{1}{2}m_2 [-2d\dot{h}\dot{\theta} \sin(\alpha_0 + \theta) \\ &\quad - 2d\dot{\theta}\dot{y}_2 \sin(\alpha_0 + \theta)] - k_\theta \theta \end{aligned}$$

$$\begin{aligned} \frac{\partial L}{\partial \theta} &= -m_1 e \dot{h} \dot{\theta} \sin(\alpha_0 + \theta) - m_2 d \dot{h} \dot{\theta} \sin(\alpha_0 + \theta) \\ &\quad - m_2 d \dot{\theta} \dot{y}_2 \sin(\alpha_0 + \theta) - k_\theta \theta \end{aligned}$$

$$\frac{\partial L}{\partial y_2} = -k_n y_2$$

$$\frac{\partial L}{\partial y_2} = -k_n y_2$$

$$\begin{aligned} \frac{d}{dt} \left( \frac{\partial L}{\partial \dot{h}} \right) &= m_1 \ddot{h} + e\ddot{\theta} m_1 \cos(\alpha_0 + \theta) - e\dot{\theta}^2 m_1 \\ &\quad \sin(\alpha_0 + \theta) + m_2 \ddot{h} + m_2 d \ddot{\theta} \cos(\alpha_0 + \theta) \\ &\quad - m_2 d \dot{\theta}^2 \sin(\alpha_0 + \theta) + m_2 \ddot{y}_2 \end{aligned}$$

$$\begin{aligned} \frac{d}{dt} \left( \frac{\partial L}{\partial \dot{\theta}} \right) &= m_1 e^2 \ddot{\theta} + m_1 e \dot{h} \cos(\alpha_0 + \theta) \\ &\quad - m_1 e \dot{h} \dot{\theta} \sin(\alpha_0 + \theta) + m_2 d^2 \ddot{\theta} \\ &\quad + m_2 d \ddot{h} \cos(\alpha_0 + \theta) - m_2 d \dot{h} \dot{\theta} \sin(\alpha_0 + \theta) \\ &\quad + m_2 d \ddot{y}_2 \cos(\alpha_0 + \theta) \\ &\quad - m_2 d \dot{y}_2 \dot{\theta} \sin(\alpha_0 + \theta) + I_{cg} \ddot{\theta} \end{aligned}$$

$$\frac{d}{dt} \left( \frac{\partial L}{\partial \dot{y}_2} \right) = m_2 \ddot{y}_2 + m_{2d} \ddot{\theta} \cos(\alpha_0 + \theta) - m_2 d \dot{\theta}^2 \sin(\alpha_0 + \theta)$$

The equations of motion of the aeroelastic system are:

$$m_1 \ddot{h} + e \ddot{\theta} m_1 \cos(\alpha_0 + \theta) - e \dot{\theta}_1^{2m} \sin(\alpha_0 + \theta) + m_2 \ddot{h} + m_{2d} \ddot{\theta} \cos(\alpha_0 + \theta) - m_{2d} \dot{\theta}^2 \sin(\alpha_0 + \theta) + m_2 \ddot{y}_2 + k_{hh} + C_h \dot{h} = -L \tag{45}$$

$$m_1 e^2 \ddot{\theta} + m_{1e} \ddot{h} \cos(\alpha_0 + \theta) - m_{1e} \dot{h} \dot{\theta} \sin(\alpha_0 + \theta) + m_{2d}^2 \ddot{\theta} + m_{2d} \ddot{h} \cos(\alpha_0 + \theta) - m_{2d} \dot{h} \dot{\theta} \sin(\alpha_0 + \theta) + m_{2d} \ddot{y}_2 \cos(\alpha_0 + \theta) - m_{2d} \dot{y}_2 \dot{\theta} \sin(\alpha_0 + \theta) + I_{cg} \ddot{\theta} + m_{1e} \dot{h} \dot{\theta} \sin(\alpha_0 + \theta) + m_{2d} \dot{\theta} \dot{h} \sin(\alpha_0 + \theta) + m_{2d} \dot{\theta} \dot{y}_2 \sin(\alpha_0 + \theta) + k_\theta \theta + C_\theta \dot{\theta} = M$$

$$m_2 \ddot{y}_2 + m_2 \ddot{h} + m_{2d} \ddot{\theta} \cos(\alpha_0 + \theta) - 2m_{2d} \dot{\theta}^2 \sin(\alpha_0 + \theta) - m_2 y_2 \dot{\theta}^2 + k_n y_2 + C_{y2} \dot{y}_2 = 0.$$

which can be written as:

$$m_1 \ddot{h} + e \ddot{\theta} m_1 \cos(\alpha_0 + \theta) - e \dot{\theta}_1^{2m} \sin(\alpha_0 + \theta) + m_2 \ddot{h} + m_{2d} \ddot{\theta} \cos(\alpha_0 + \theta) - m_{2d} \dot{\theta}^2 \sin(\alpha_0 + \theta) + m_2 \ddot{y}_2 + k_{h0} h + k_{h1} h^2 + k_{h2} h^3 + C_h \dot{h} = -L$$

$$m_1 e^2 \ddot{\theta} + m_{1e} \ddot{h} \cos(\alpha_0 + \theta) + m_{2d}^2 \ddot{\theta} m_{2d} \ddot{h} \cos(\alpha_0 + \theta) + m_{2d} \ddot{y}_2 \cos(\alpha_0 + \theta) + I_{cg} \ddot{\theta} + k_{\theta_0} \theta + k_{\theta_1} \theta^2 + k_{\theta_2} \theta^3 + C_\theta \dot{\theta} = M$$

$$m_2 \ddot{y}_2 + m_2 \ddot{h} + m_{2d} \ddot{\theta} \cos(\alpha_0 + \theta) - 2m_{2d} \dot{\theta}^2 \sin(\alpha_0 + \theta) + k_{n_0} y_2 + k_{n_1} y_2^2 + k_{n_2} y_2^3 + C_{y2} \dot{y}_2 = 0.$$

References

1. Lee, Y.S., Vakakis, A.F., Bergman, L.A., McFarland, D.M., Kerschen, G.: Passive suppression of aeroelastic instabilities of in-flow wings by targeted energy transfers to lightweight essentially nonlinear attachments. In: International Forum on Aeroelasticity and Structural Dynamics, Stockholm (2007)
2. Jiang, X., McFarland, D.M., Bergman, L.A., Vakakis, A.F.: Steady state passive nonlinear energy pumping in coupled oscillators: theoretical and experimental results. *Nonlinear Dyn.* **33**, 87–102 (2003)
3. Malatkar, P., Nayfeh, A.H.: Steady-state dynamics of a linear structure weakly coupled to an essentially nonlinear oscillator. *Nonlinear Dyn.* **47**, 167–179 (2006)
4. Mehmood, A., Nayfeh, A.H., Hajj, M.R.: Effects of a nonlinear energy sink (NES) on vortex-induced vibrations of a circular cylinder. *Nonlinear Dyn.* **77**, 667–680 (2014)
5. Guo, H., Chen, Y., Tian-zhi, Y.: Limit cycle oscillation suppression of 2-DOF airfoil using nonlinear energy sink. *Appl. Math. Mech.* **34**, 1277–1290 (2013)
6. Fung, Y.C.: An Introduction to the Theory of Aeroelasticity. Dover Publications, New York (1993)
7. Abdelkefi, A., Vasconcellos, R., Marques, F., Hajj, M.R.: Modeling and identification of freeplay nonlinearity. *J. Sound Vib.* **331**, 1898–1907 (2012)
8. Strganac, T.W., Ko, J., Thompson, D.E.: Identification and control of limit cycle oscillations in aeroelastic systems. *J. Guid. Control Dyn.* **23**(6), 1127–1133 (2000)
9. Nayfeh, A.H.: The Method of Normal Forms. Wiley-VCH, London (2011)
10. Nayfeh, A.H., Balachandran, B.: Applied Nonlinear Dynamics. Wiley, London (1994)